# Numerical simulations of spatially developing, accelerating boundary layers

Ugo Piomelli[1, a)] and Junlin Yuan[1, b)]

*Department of Mechanical and Materials Engineering, Queen's University, Kingston (Canada)*

(Dated: 15 June 2013)

We present results of direct and large-eddy simulations of spatially developing boundary layers subjected to favorable pressure gradient (FPG), strong enough to cause relaminarization. The numerical results compare well with experimental data. Visualization of the flow structures shows the well-known stabilization of the streaks, the re-orientation of outer layer vortices in the streamwise direction, and the appearance of turbulent spots in the re-transition region. Both instantaneous visualizations and turbulent statistics highlight the significant damping of wall-normal and spanwise fluctuations. The fast component of the pressure fluctuations appears to be the main driver of this process, contributing to reduce pressure fluctuations and, as a consequence, the energy redistribution term in the Reynolds stress budgets. The streamwise stresses, in whose budget a separate production term plays a role, do not decay but remain frozen at their upstream value. The decrease of wall-normal fluctuations appears to be the main cause of the inner-layer stabilization, consistent with the picture of the turbulence-generation cycle proposed, for equilibrium wall-bounded flows, by Jimenez and Pinelli [J. Fluid Mech. 389, 335 (1999)].

[a)]Electronic mail: ugo@me.queensu.ca

[b)]Electronic mail: junlin.yuan@queensu.ca

## I. INTRODUCTION

The canonical turbulent boundary layer occurs on a flat plate in which the mean streamwise pressure gradient is zero. In real applications, however, freestream acceleration or deceleration are commonly encountered. A favorable pressure gradient (FPG), which results in freestream acceleration, is present in many engineering applications: the leading-edge region of an airfoil, for instance. Boundary layers in FPG may present unusual features: although the kinetic energy of the mean flow is increased by the acceleration of the free stream, turbulence may become less vigorous and the flow may even revert to a laminar state. Understanding the dynamics of this relaminarization process is important, and FPG boundary layers have been studied since the 1960s. The articles by Narasimha and Sreenivasan[1] and Sreenivasan[2] highlight many of the questions that are still relevant today in relaminarizing flows.

The favorable pressure gradient can be characterized by the the acceleration parameter $K = (\nu/U_\infty^2)dU_\infty/dx$ (where $\nu$ is the kinematic viscosity and $U_\infty$ the freestream velocity). The simplest accelerating boundary layer is the "sink flow" that occurs in a two-dimensional convergent channel. In sink flows $K$ is constant with streamwise distance $x$. An exact solution can be found in laminar conditions,[3] whereas in turbulent flow experimental studies show that a self-similar state is reached as the flow approaches the sink.[4,5] For strong acceleration ($K$ between 2.5 and $3 \times 10^{-6}$) turbulence cannot be sustained, and the flow relaminarizes.[5–7]

In reality, since the FPG cannot be maintained for an infinite distance, a region of FPG and streamwise acceleration is followed by one with constant or adverse pressure gradient, and full re-laminarization may not occur; the pressure gradient may leave the flow in a "laminarescent" state.[2] Once the FPG ends, the flow reverts to its turbulent state; the re-transition process depends critically on the state of the flow in the FPG region. The (sudden or gradual) imposition of the pressure gradient

perturbs turbulence from an equilibrium state, and the response of the flow depends on the spatial distribution of $K$. The value of $K$ reached during the acceleration, and the distance for which this value is maintained, determine the relaminarization and retransition process.

Launder[8] was among the first to observe experimentally relaminarization in a converging nozzle. In two papers with Jones,[4,5] which included measurements only published as an internal MIT report,[9] sink flows are discussed, including relaminarizing cases. For values of $K = o(10^6)$ no logarithmic region is observed. An increase of the energy at low wave-numbers in the near-wall region indicates that the longitudinal length scales of the flow increase. Launder[9] also observed that the turbulence does not vanish, but an increasing fraction of it plays a passive role in the boundary-layer development.

Badri Narayanan and Ramjee[6] performed a series of experiments on accelerating flows, both in equilibrium (sink flows) and spatially developing cases. The inflow boundary layer was always turbulent. They observed relaminarization of the flow, beginning near the wall and moving outward towards the freestream; they conjecture that the breakdown of the log law is due to thickening of the viscous sublayer, and is preceded by a decrease of the burst frequency. A correlation between burst frequency and $K$ was also observed by Kline *et al.*[10]

Blackwelder and Kovasznay[11] noted that, along streamlines, the Reynolds stresses remain constant, at least away from the wall; they also observed a smaller, but significant, level of the shear stress $\langle u'v' \rangle$ (where $\langle \cdot \rangle$ indicates time averaging, and a prime denotes a fluctuating quantity). They also observed a thickening of the viscous sublayer and observed, based on space-time correlations, that the large structures are not significantly modified.

Several researchers[6,12–14] have proposed criteria for relaminarization. Narasimha and Sreenivasan[1] point out that many of these criteria are related to the Reynolds

number; this implies that relaminarization is driven by an excess of dissipation, whereas experimental data (Badri Narayanan *et al.*,[15] reported in Ref. 1) show that production remains greater than dissipation in the acceleration region. Narasimha and Sreenivasan[14] argue that the Reynolds stresses are advected from the zero-pressure-gradient region, and that pressure forces dominate over the "frozen" Reynolds stresses in the outer layer. They also observe that the Reynolds shear stresses maintain their correlation in the acceleration region.

In a series of paper, McEligot and coworkers[16–19] studied the flow in a laterally converging duct. Their configuration differed from the others discussed here in that in their case the acceleration was not associated with a mean wall-normal velocity, $V_\infty$, directed towards the wall. Some of their conclusions, however, are consistent with the results observed in sink-flow boundary layers and, to some extent, in spatially developing ones as well. By applying the Variable-Interval Time-Averaging (VITA) technique to the oscillating wall stress they observed that the burst frequency is very sensitive to the acceleration, decreasing as $K$ increases.[17] The duration of the sweeps, on the other hand, increases with acceleration. McEligot and Eckelman[18] measured the wall-normal fluctuation in the viscous layer and observed that it decreases as the pressure gradient increases, and that transport of momentum also decreases when the acceleration is strong.

Fernholz and Warnack[20] and Warnack and Fernholz[21] performed experiments on axisymmetric boundary layers subjected to acceleration. Their studies covered a wide range of acceleration parameters ($0 < K < 4 \times 10^{-6}$) and Reynolds numbers ($860 < Re_\theta < 5,800$). They considered both mild acceleration that resulted in an equilibrium boundary layer,[20] and strong acceleration.[21] In the high-acceleration cases[21] the streamwise Reynolds stresses increase in the near-wall region, while they initially decrease and then begin increasing in the outer region. The shear stresses also initially decrease and later recover and increase. The correlation coefficient be-

tween streamwise and wall-normal velocity fluctuations increases in the acceleration region. The integral scale increases as the near-wall vortices are stretched in the streamwise direction, but are only slightly smaller in the wall-normal direction.

Escudier *et al.*[22] also found, in an experimental study of a strongly accelerated boundary layer, that the streamwise fluctuations in the outer layer are frozen. They observed that the intermittency goes to zero in the region of high acceleration, indicating a fundamental change in the turbulence structure.

Bourassa and Thomas[23], more recently, performed experiments that support the dual-layer characteristic during re-laminarization: turbulent production in the inner region decreased much faster than in the outer region as the flow was accelerated; also, the Reynolds-stress correlation was most strongly affected in the near-wall region where it decreased and reached very small values at locations associated with relaminarization; in the outer layer high correlations were maintained due to the streamwise straining of vortical structures that originated in the upstream flow. The stabilizing effect of acceleration on near-wall streaky structures was explained as a combined effect of reductions of both the wall-normal and spanwise vorticities: the reduction of the wall-normal component was due to larger spanwise separation of streaks, while acceleration led to reduced spanwise vorticity. This was consistent with the decrease in the number of ejections; the surviving ejections became strong due to the straining of streamwise vortices. The wall-normal motions between the inner and outer layers were found to be dominated by ejections and third-quadrant ($u' < 0,\ v' < 0$) events in regions of high acceleration; third-quadrant events reduce the Reynolds stress correlation and the wall-normal transport of momentum, and cause a lower friction coefficient and a thicker viscous sublayer.

Piomelli *et al.*[24] performed large-eddy simulations (LES) of a spatially developing boundary layer, with two freestream-velocity distributions. They described the kinematic effects of the acceleration on the turbulent eddies, observing that the near-

wall streaks become more elongated and show fewer undulations. From instantaneous flow visualization they conjectured that the vortex-stretching and reorientation due to the streamwise velocity gradient is the main mechanism driving the topology of the vortical structures.

In a follow-up study, De Prisco *et al.*[25] observed both re-laminarization mechanisms that were present in experiments: (1) a stabilized inner layer, and a frozen and isolated outer layer, and (2) a strong role of the outer region, characterized by incursions of irrotational fluid from the outer layer, and strong ejections of inner-layer fluid into the outer layer. It was not clear, however, which mechanism dominated. Once the stabilizing influence of the pressure gradient was removed, the re-transition occurred very rapidly, following a process similar to by-pass transition due to high freestream turbulence. They also observed that, in the outer layer, large coherent structures were oriented in the streamwise direction, forming a well-mixed layer, where turbulent production decreased, and the frozen turbulence was advected downstream. In the inner layer, the flow became more orderly, with longer, more two-dimensional streaky structures and decreased bursting frequency in the re-laminarization region.

Large-scale structures were also studied experimentally by Harun *et al.*[26] They pointed out that the decrease of outer-layer turbulent intensity in the accelerating boundary layer is due to a combined effect of mean-shear decrease and less energetical large-scale activities. However, the similar spectral distribution of energy in the wake region suggested that the large-scale motions did not change in character.

Despite the decades of study, some of the mechanisms involved in the re-laminarization of the accelerating turbulent boundary layer are still unclear. While the inner-layer turbulence is stabilized and undergoes a process of laminarization, in the outer-layer the statistics do not adapt to the acceleration and the turbulent structures are strained in the streamwise direction; after the acceleration is completed,

the flow quickly re-transitions to an equilibrium boundary layer. Several questions are still open; among them are: (1) Is the outer layer turbulence passively frozen or does it play a role in the re-laminarization phenomenon? (2) How do the inner and outer layers interact during and after the acceleration? (3) Is the inner-outer interaction promoted or attenuated by acceleration? In this paper, using the results of new direct and large-eddy simulations of this flow, we will attempt to review and illustrate some of these issues, and answer some of the open questions.

## II. PROBLEM FORMULATION

### A. Governing equations and numerical method

The incompressible flow of a Newtonian fluid is governed by the equations of conservation of mass and momentum:

$$\frac{\partial u_i}{\partial x_i} = 0, \tag{1}$$

$$\frac{\partial u_i}{\partial t} + \frac{\partial}{\partial x_j}(u_i u_j) = \frac{\partial P}{\partial x_i} + \frac{1}{Re}\nabla^2 u_i. \tag{2}$$

The equations have been made dimensionless using a reference velocity and length, $U_r$ and $L_r$ (which will be specified later). $x_1$, $x_2$ and $x_3$ (or $x$, $y$ and $z$) are, respectively, the streamwise, wall-normal and spanwise directions, and $u_i$ (or $u$, $v$ and $w$) are the velocity components in those directions; $P = p/\rho$ is the modified pressure, $\rho$ the density and $Re = U_r L_r/\nu$ the Reynolds number. In Large-Eddy Simulations (LES), (1-2) are solved for filtered quantities, and the divergence of the sub-grid stress tensor, $\tau_{ij} = \overline{u_i u_j} - \overline{u}_i \overline{u}_j$, appears on the right hand side of the momentum equation. In the present study, $\tau_{ij}$ was modeled using a dynamic eddy-viscosity model,[27,28] in which the coefficient was adjusted using the Lagrangian-Averaging procedure.[29]

The governing equations were discretized using second-order central differences

on a staggered grid, and integrated using a fractional step method.[30,31] The spatial discretization of the convective terms conserves momentum and energy discretely.[32] All terms were advanced explicitly in time using a three-step, second-order Runge-Kutta method, except for the diffusive term in $y$, which was advanced implicitly using a second-order Crank-Nicolson method. The Poisson equation was solved directly by Fourier expansion in the spanwise direction (in which the spacing is uniform) followed by direct inversion of the resulting penta-diagonal matrix at each wave-number. The code is parallelized using MPI, and has ben validated extensively for a variety of turbulent flows.[33–35]

Periodic boundary conditions were used in the spanwise direction. A variable freestream velocity $U_\infty(x)$ was imposed on the top boundary of the domain, and $V_\infty$ was obtained from conservation of mass.[36] The velocity fluctuations were obtained by requiring that the vorticity in the freestream is zero. An unsteady inflow boundary condition was obtained using the recycling/rescaling method,[36] while a convective outflow boundary condition was used at the domain outlet.[37]

### B. Simulation parameters

In all calculations the reference quantities are the displacement thickness $\delta^*$ and the freestream velocity, measured at a location downstream of the recycling station. They are referred to as $\delta_o^*$ and $U_o$ and the distances are rescaled so that the reference location corresponds to $x = 0$. The computational domains for the DNS extended between $-50 < x/\delta_o^* < 450$, and the spanwise and wall-normal domain sizes were $17\delta_o^*$. In the LES, the dimensions were, respectively $-45 < x/\delta_o^* < 511$, and $28\delta_o^*$ in $y$ and $28\delta_o^*$ in $z$. The number of grid points used, as well as other simulation parameters, is shown in Table I. Since the velocity increased by a factor of almost three in the streamwise direction, the resolution in wall units becomes progressively

TABLE I. Summary of simulation parameters.

| Case | $K_{max}$ | $Re_{\theta,o}$ | $h_s/\delta_o^*$ | Grid |
|---|---|---|---|---|
| DNS1 | $8 \times 10^{-6}$ | 458 | 0 | 4096×257×384 |
| LES1s | $8 \times 10^{-6}$ | 454 | 0 | 1024×144×128 |
| LES1h2 | $8 \times 10^{-6}$ | 452 | 0.2 | 1024×170×128 |
| LES1h4 | $8 \times 10^{-6}$ | 456 | 0.4 | 1024×170×128 |
| LES3s | $4 \times 10^{-6}$ | 737 | 0 | 1792×159×256 |

coarser. Care was taken to ensure that, even near the outflow, the grid was sufficiently fine to resolve all the important turbulent eddies. For the DNS the grid spacing at $x/\delta_o^* = 0$ was $\Delta x^+ \simeq 3.7$, $\Delta z^+ \simeq 1.6$, while at $x/\delta_o^* = 400$, $\Delta x^+ \simeq 8.8$ and $\Delta z^+ \simeq 3.8$. For the low-$Re$ LES, $\Delta x^+$ and $\Delta z^+$ are 18 and 6 at $x = 0$ and 70 and 16 at $x/\delta_o^* = 400$, while for the high-$Re$ LES they are 27 and 5 at $x/\delta_o^* = 0$, 68 and 13 at 400. Even the marginal LES is fine enough that we expect to resolve the near-wall eddies with very good accuracy.

## III. RESULTS

### A. Turbulence statistics

Figure 1 shows contours of mean $U$ and $V$ in the useful region, together with streamwise profiles of $U_\infty$ and $K$, for case DNS1. We observe the significant increase (by nearly three times) of the mean streamwise velocity, the relatively low wall-normal velocity required to accelerate the flow (less than 10% of the streamwise one), the thinning of the boundary layer, which reaches its minimum where the acceleration parameter is maximum and (as will be shown later) the wall stress

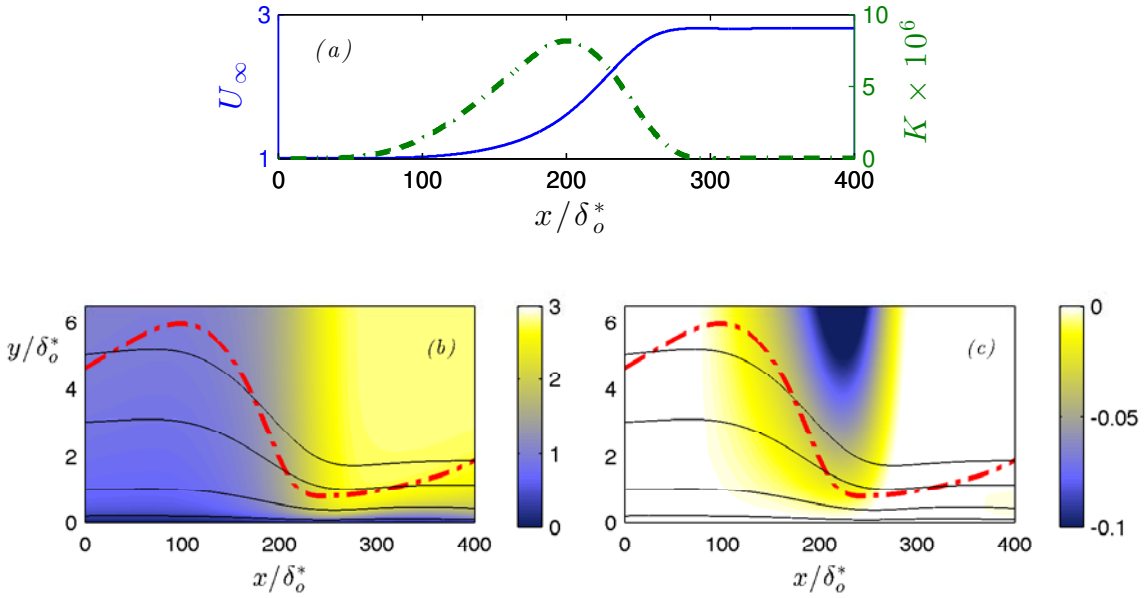


FIG. 1. Case DNS1. *(a)* —— Freestream velocity $U_\infty$ and - - - acceleration parameter $K$. *(b)* Contours of $U/U_o$. *(c)* Contours of $V/U_o$. —·—: $\delta_{95}$. The thin lines are representative streamlines.

begins to decrease, indicating flow re-laminarization. It is also interesting to note that, as the boundary layer becomes thinner, several streamlines are de-trained from the boundary layer into the irrotational region.

Since there is no data available for model validation at the low $Re$, we have performed simulations at a higher Reynolds number matching the experiments of Ref. 21. Figures 2*(a)* and *(b)* show the acceleration parameter and freestream velocity for the low-$Re$ DNS (Case DNS1) and the high-$Re$ LES (Case LES3). The momentum-thickness Reynolds number $Re_\theta = U_\infty \theta/\nu$, with

$$\theta = \int_0^\infty \frac{U}{U_\infty}\left(1 - \frac{U}{U_\infty}\right) dy \tag{3}$$

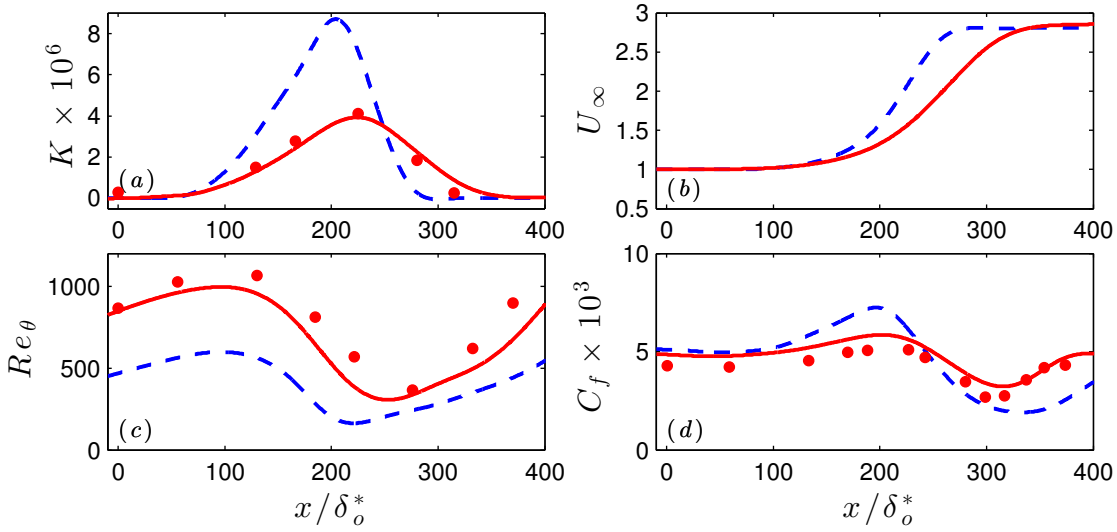


FIG. 2. Boundary layer parameters. *(a)* Acceleration parameter $K$; *(b)* Freestream velocity $U_\infty$; *(c)* Reynolds number $Re_\theta$; *(d)* Skin-friction coefficient $C_f$. - - - DNS1, —— LES3, • Experiment.[21]

is shown in Figure 2*(c)*, and the skin-friction coefficient.

$$C_f = \frac{\tau_w}{\rho U_\infty^2/2} \tag{4}$$

in Figure 2*(d)*. We obtained very good agreement between the LES and the experiments (a comparison of mean velocities and Reynolds stresses will follow). While $Re_\theta$ begins decreasing as soon as the acceleration increases (the decrease of $\theta$ being more significant than the increase of $U_\infty$), $C_f$ does not begin to decrease until the point where $K$ is maximum. This is an indication of a difference in the response of inner and outer layers to the acceleration. $C_f$ continues to decrease until $U_\infty$ becomes constant, at which point it increases rapidly and, after a small overshoot, settles to a new equilibrium. This behaviour is reminiscent of transition induced by free-stream noise.

The mean velocity profiles in wall units are shown in Figure 3. The logarithmic

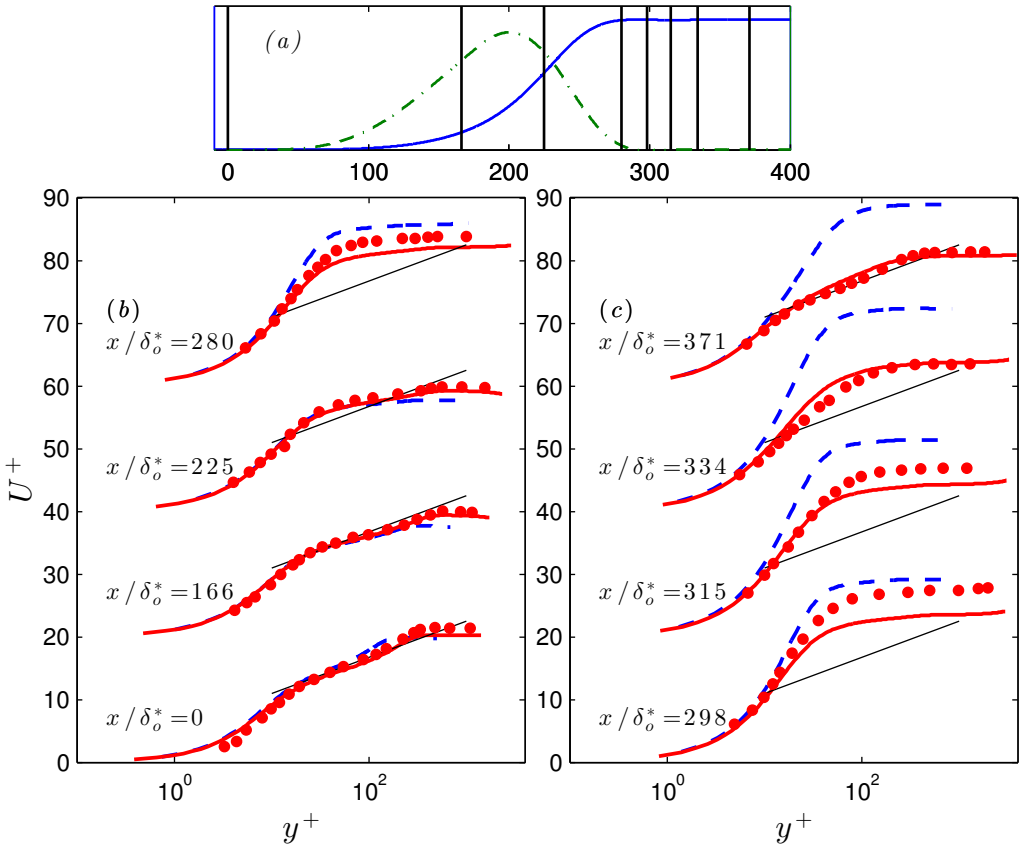


FIG. 3. *(a)* Location of the mean profiles (vertical lines) relative to —— $U_\infty/U_o$ and —·— $K$. The mean-velocity profiles in wall units are shown for *(b)* $0 \le x/\delta_o^* \le 280$ and *(c)* $280 \le x/\delta_o^* \le 371$. Each profile is shifted upwards by 20 units for clarity. - - - DNS1, —— LES3, • Experiment.[21]

layer follows the standard law, $U^+ = 2.5 \log y^+ + 5.2$, near the inflow, but, as the acceleration becomes significant, the slope of the logarithmic region decreases (a well-known effect of acceleration[7]). In the region of flow re-laminarization a laminar-like behavior can be observed, with a longer linear region and the profile extending above the logarithmic law. A thick layer with $\partial U/\partial y \simeq 0$ can also be observed;

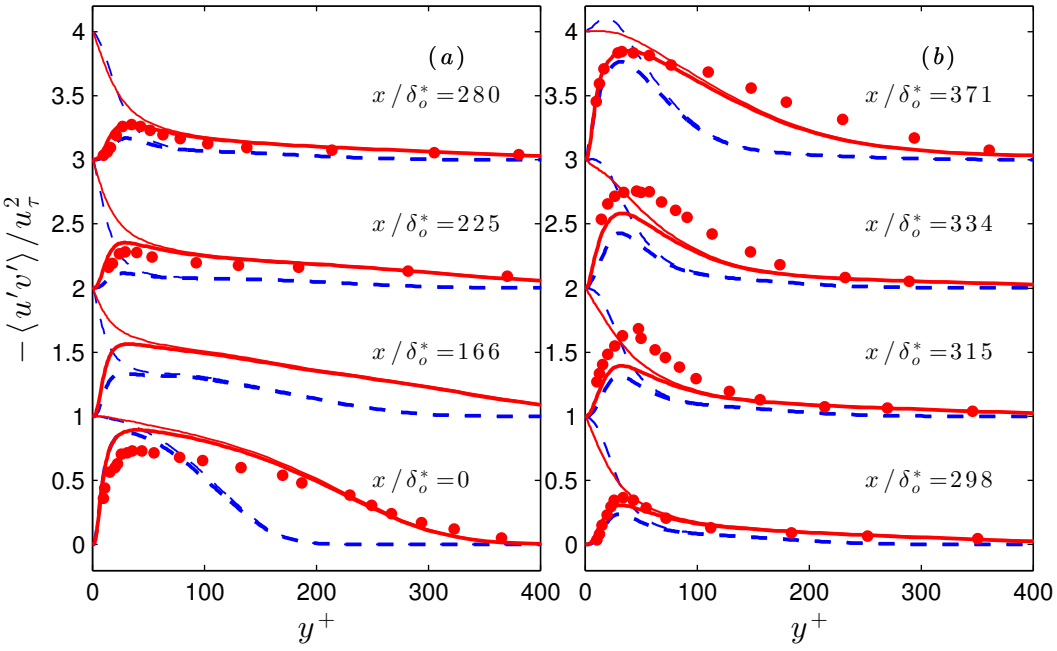


FIG. 4. Shear-stress profiles in wall units for *(a)* $0 \leq x/\delta_o^* \leq 280$ and *(b)* $280 \leq x/\delta_o^* \leq 371$. Each profile is shifted upwards by 1 unit for clarity. See Figure 3 for locations of the profiles. --- DNS1, ——— LES3, • Experiment[21] (Reynolds stress only). Thick lines: $-\langle u'v' \rangle$; thin lines: total shear stress.

in this region, production is very low, as also observed by Warnack and Fernholz[21] and Bourassa and Thomas.[23] The agreement between the LES and the experiment is, again, very good. By $x/\delta_o^* \simeq 370$ the high-$Re$ calculation has returned to an equilibrium configuration with the standard logarithmic behavior, while the low-$Re$ case still has a more laminar-like behavior.

Figure 4 shows the shear stresses in inner units; for the LES, the subgrid-scale contribution is included in $-\langle u'v' \rangle$. The total shear stress (sum of resolved, SGS—if present—and viscous) is also shown in the figure. The LES is in good agreement with the experimental results. The Reynolds stresses decrease significantly in the region of

peak $K$; the maximum $-\langle u'v' \rangle$ decreases by a factor of three in the low-$Re$ case, and has not recovered yet by the end of the domain. In the higher-$Re$ case the deviation from the equilibrium profile is less significant, and lasts for a shorter distance. Note in particular the change of shape of the curve: while in equilibrium the Reynolds stress is nearly constant for $10 < y^+ < 100$ (corresponding to logarithmic behavior), in the acceleration and relaminarization region the profiles have a sharper peak, and the total stress has an upward concavity. The same phenomenon has been observed in sink flow simulations (see, for example, Figure 5 in Ref. 7), and, in developing FPG boundary layers.[21] As the acceleration is removed, the viscous region adjusts first. In the buffer layer, however, a local overshoot in the total stress persists for some distance; this is most evident at the last location for the DNS, but is also visible at $x/\delta_o^* = 334$ in the LES data (in the high-$Re$ case the flow is less perturbed, and by $x/\delta_o^* = 371$ it has nearly returned to equilibrium). A similar overshoot was observed by Wu and Moin[38] in the late transitional stages of a boundary layer with freestream turbulence.

Contours of the Reynolds stresses for the low-$Re$ DNS are shown in Figure 5. While the streamwise stresses $\langle u'u' \rangle$ decrease slightly in the acceleration region, the wall-normal ones, $\langle v'v' \rangle$, are much more significantly damped by the acceleration. In the region $230 < x/\delta_o^* < 320$, in particular, the wall-normal stresses are negligible everywhere inside the boundary layer, and are non-zero only far from the wall, as a consequence of the advection of inactive eddies from upstream.

The damping of the wall-normal fluctuations can be visualized better if the stream-function

$$\psi(x, y) = \int_0^y U(x, y')dy' \tag{5}$$

is used as ordinate in the contour plots.[11] In these coordinates, horizontal lines correspond to mean-flow streamlines. Figure 6 shows the Reynolds stresses plotted in this

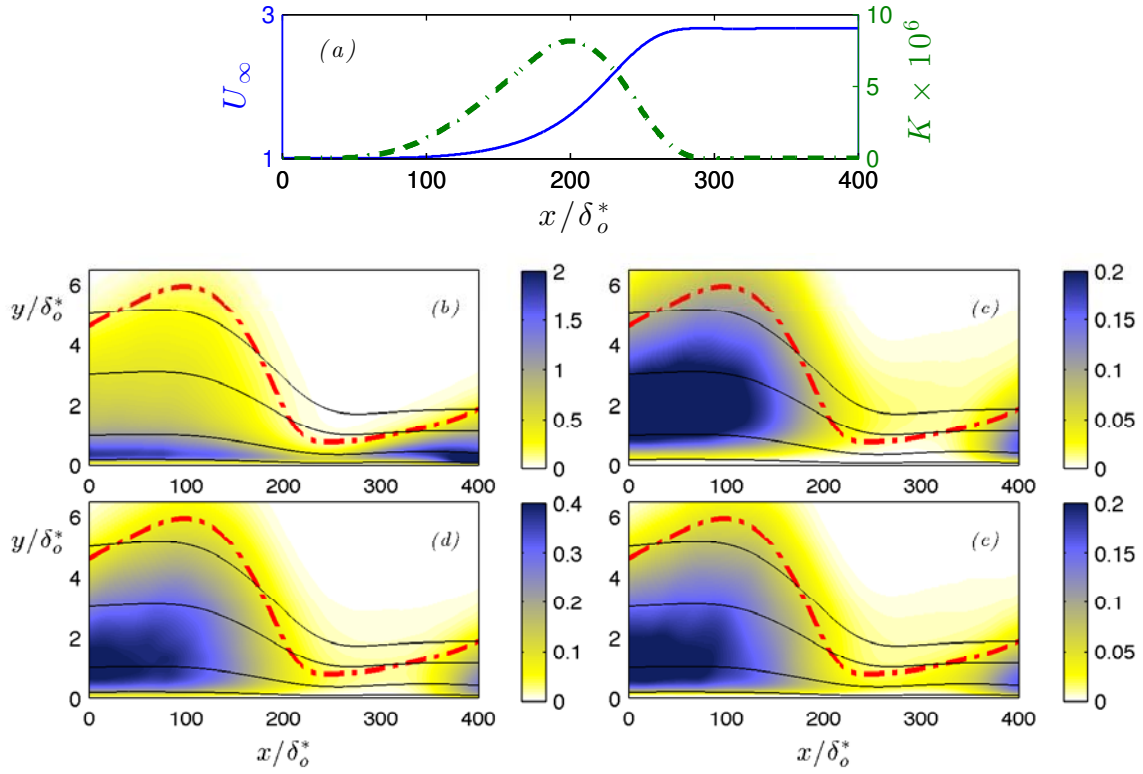


FIG. 5. Case DNS1. *(a)* —— Freestream velocity $U_\infty$ and - - - acceleration parameter $K$. *(b)* $100\langle u'u'\rangle$; *(c)* $100\langle v'v'\rangle$; *(d)* $100\langle w'w'\rangle$; *(e)* $-100\langle u'v'\rangle$. —·—: $\delta_{95}$; the thin lines are representative streamlines.

manner. Better to illustrate the changes that fluid particles experience, the stresses have been normalized by their value at the reference location $x/\delta_o^* = 0$, along the same streamline (*i.e.*, at the same value of $\psi$). The streamwise normal stresses $\langle u'u'\rangle$ near the wall remain constant up to $x/\delta_o^* \simeq 200$ (the location of maximum $K$), and then begin to increase; the flow, however, does not catch up to the freestream acceleration, resulting in the decrease of $\langle u'u'\rangle/U_\infty^2$ seen in Figure 5. In the outer layer $\langle u'u'\rangle$ begins to decrease along streamlines as soon as the pressure gradient becomes significant. The decrease is more significant as one moves towards the freestream

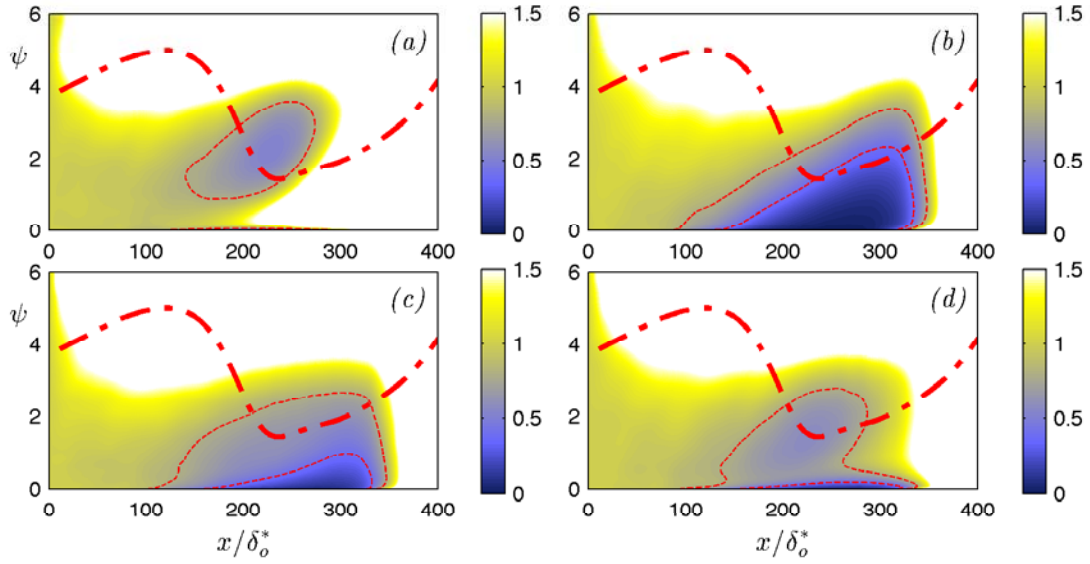


FIG. 6. Case DNS1. Contours of the Reynolds stresses, normalized by their value at the reference location $x/\delta_o^* = 0$, in stream-function coordinates. *(a)* $\langle u'u' \rangle$; *(b)* $\langle v'v' \rangle$; *(c)* $\langle w'w' \rangle$; *(d)* $-\langle u'v' \rangle$. —·—: $\delta_{95}$; the dashed lines show contour levels 0.8 and 0.4.

(as also observed by Escudier *et al.*[22]) and for streamlines that are de-trained out of the boundary layer. The damping of streamwise fluctuations appears to be an outer-layer phenomenon, and may be related to the changes in the shape of the turbulent structures in this region, and to the decrease of production to the creation of a well-mixed layer with $\partial U/\partial y \simeq 0$.

The wall-normal stresses $\langle v'v' \rangle$ and the spanwise ones $\langle w'w' \rangle$ have a very different behavior: throughout the flow, they decrease in absolute magnitude (not only with respect to the freestream velocity). The decrease begins earlier for streamlines close to the wall, and then propagates outwards towards the freestream. The shear stress also decrease as a result of the damping of the wall-normal fluctuations and not (as in other flows) by a decorrelation of the $u'$ and $v'$ fluctuations, which actually increases

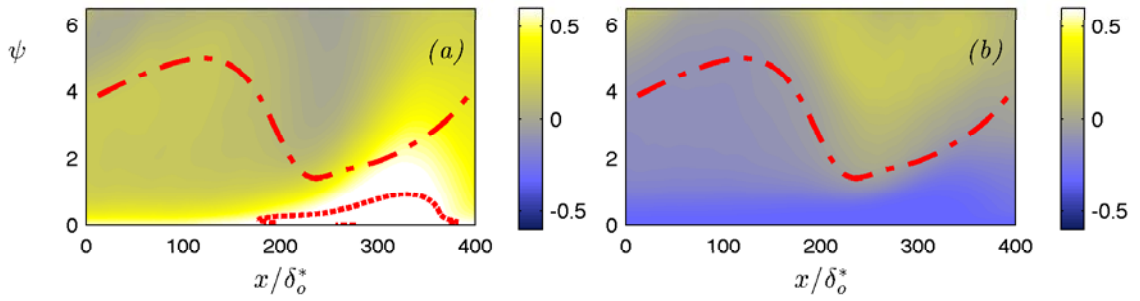


FIG. 7. Case DNS1. Contours of the Reynolds-stress anisotropy.*(a)* $b_11$; *(b)* $b_{22}$ The dashed line shows contour level 0.6. The dash-dot line shows $\delta_{95}$.

in the relaminarization region, as observed by Warnack and Fernholz.[21] The different behavior of the streamwise, wall-normal and spanwise stresses are due to the different generation mechanisms that occur in their respective budget equations, and will be discussed later in Section III D.

The Reynolds-stress anisotropy is defined as

$$b_{ij} = \frac{\langle u_i u_j \rangle}{\langle u_k u_k \rangle} - \frac{\delta_{ij}}{3}. \tag{6}$$

In the limit of one-dimensional turbulence, the relevant component of the normal anisotropy components, $b_{\alpha\alpha}$ (no summation on Greek indices), is 2/3, while the other normal components are equal to $-1/3$. The contours presented in Figure 7, show an extended region in which $b_{11} > 0.6$. This is another symptom of the disruption of the structure of the eddies caused by the acceleration.

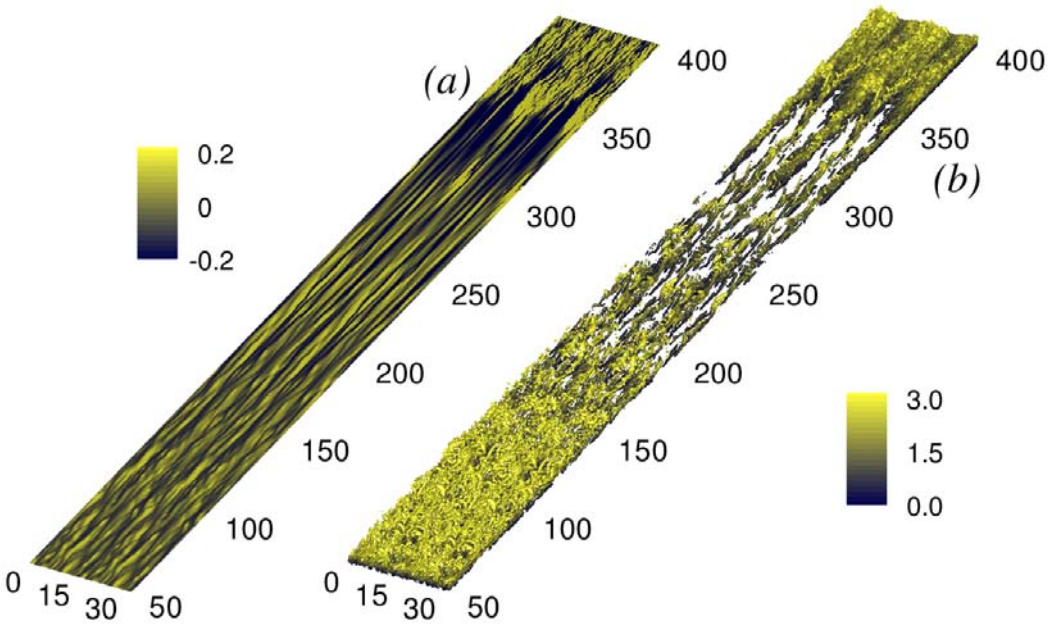


FIG. 8. Instantaneous flow visualization. *(a)* Contours of streamwise velocity fluctuations, $u'$, in a plane parallel to the wall, and *(b)* isosurfaces of $Q$ coloured by $U/U_\infty$. The data has been replicated once in the spanwise direction for clarity.

## B. Turbulent structures

Figure 8 shows contours of streamwise velocity fluctuations, $u'$, in a plane parallel to the wall, and isosurfaces of the second-invariant of the velocity gradient tensor,

$$Q = -\frac{1}{2}\frac{\partial u_i}{\partial x_j}\frac{\partial u_j}{\partial x_i}. \tag{7}$$

This figure shows the usual boundary-layer structure in the zero-pressure-gradient region near the inlet, characterized by alternating low- and high-speed streakes. The streaks become more elongated in the high-acceleration region, concomitant with less frequent occurrence of the outer-layer eddies (Figure 8*(b)*).[24,25] When the pressure gradient is released, the flow re-transitions. The transition process is characterizd by

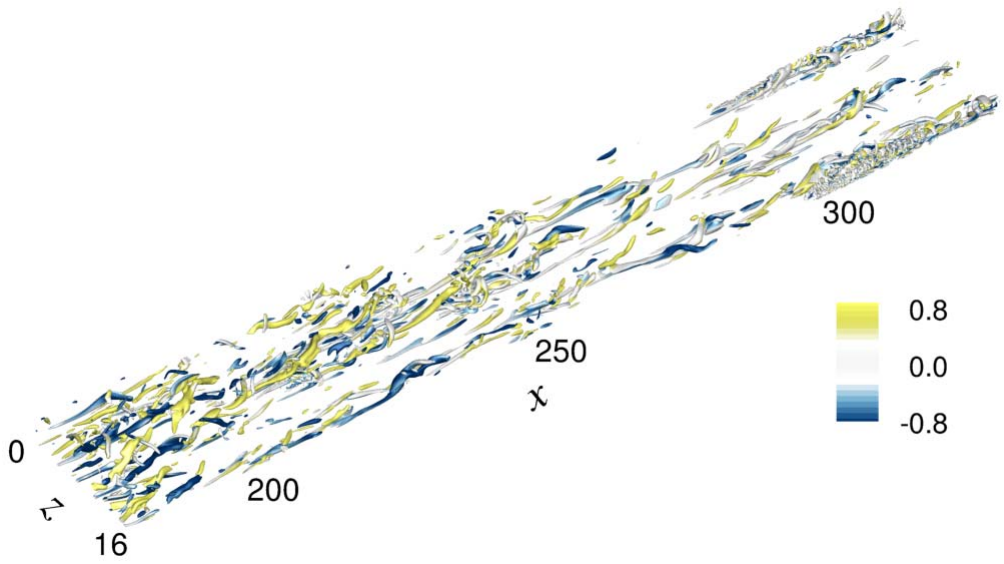


FIG. 9. Instantaneous flow visualization of the high-pressure-gradient region. Isosurfaces of $Q$ coloured by $\omega'_x/\omega'$.

the appearance of turbulent spots with a characteristic $\Lambda$ shape, which grow as they are advected downstream, and eventually merge to form a fully turbulent region, for $x/\delta_o^* > 400$. This picture is another indication that the flow retransitions in a process similar to bypass transition induced by high-level free-stream turbulence. The $C_f$ development, the overshoot in the shear stresses near the wall, and the appearance of turbulent spots are strong indications of this.

Figure 9 shows the re-laminarization region in detail. Here, the iso-surfaces of $Q$ are coloured by $\omega'_x/\omega'$, where $\omega'_x$ is the fluctuating streamwise vorticity, and

$$\omega' = (\omega'_i\omega'_i)^{1/2}\,; \qquad \omega'_i = \varepsilon_{ijk}\frac{\partial u'_j}{\partial x_k}. \tag{8}$$

Initially, for $x/\delta_o^* \simeq 200$, we observe quasi-streamwise vortices, eddies that are inclined at approximately $45^o$ to the wall, and horseshoe heads. As the acceleration becomes significant reorientation tends to align the vortices in the $x$-direction, as

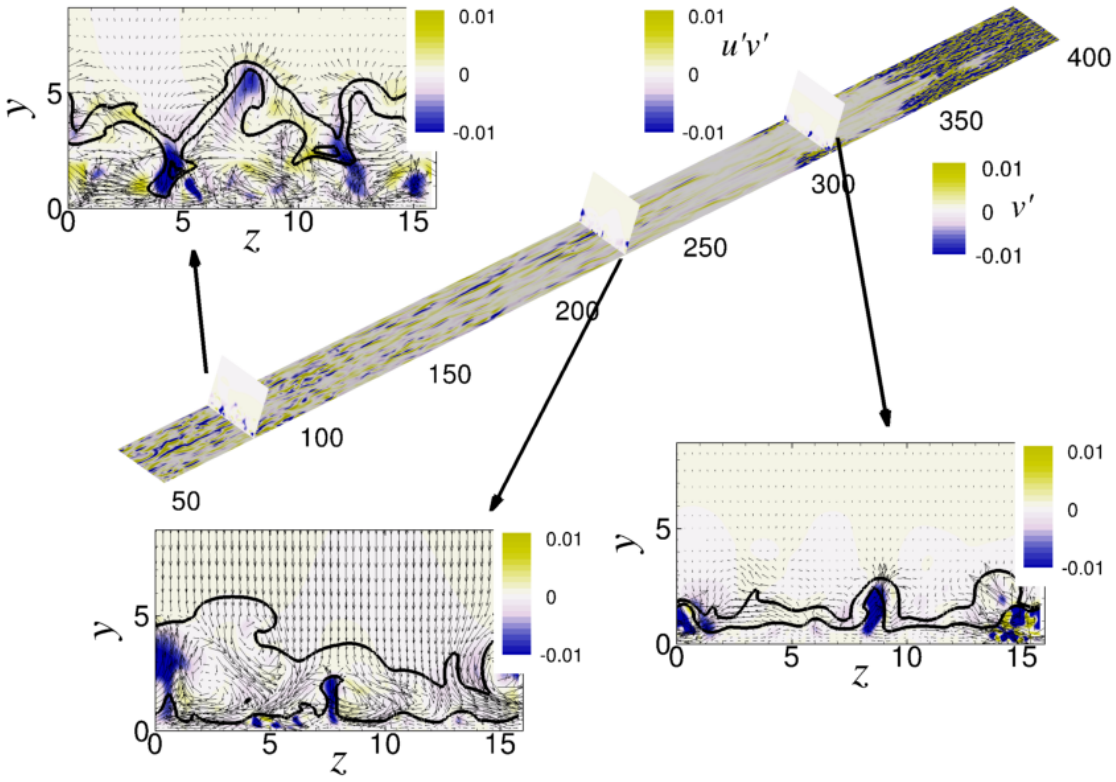


FIG. 10. Contours of $v'$ in a plane parallel to the wall, and contours of the $u'v'$ superposed on velocity vectors in the cross-planes ($yz$-planes). The two thick lines indicate the 90% and 98% boundary-layer thicknesses.

first observed by Piomelli *et al.*[24] Around $x/\delta_o^* \simeq 250$ most of the vortices have taken this alignment (we observe only rarely the hairpin heads that can be seen in the equilibrium region), and the vorticity is mostly in the $x$ component. Significant $y$-vorticity still exists: the spanwise gradient of $u'$ is not small, since the streaky structures shown in Figure 8 are fairly stable, but still quite thin.

Figure 10 shows wall-normal velocity-fluctuation contours in a plane parallel to the wall, and also contours of the $u'v'$ correlation and velocity vectors in three $yz$-planes: one in the zero-pressure-gradient region, one where the acceleration is strong, and

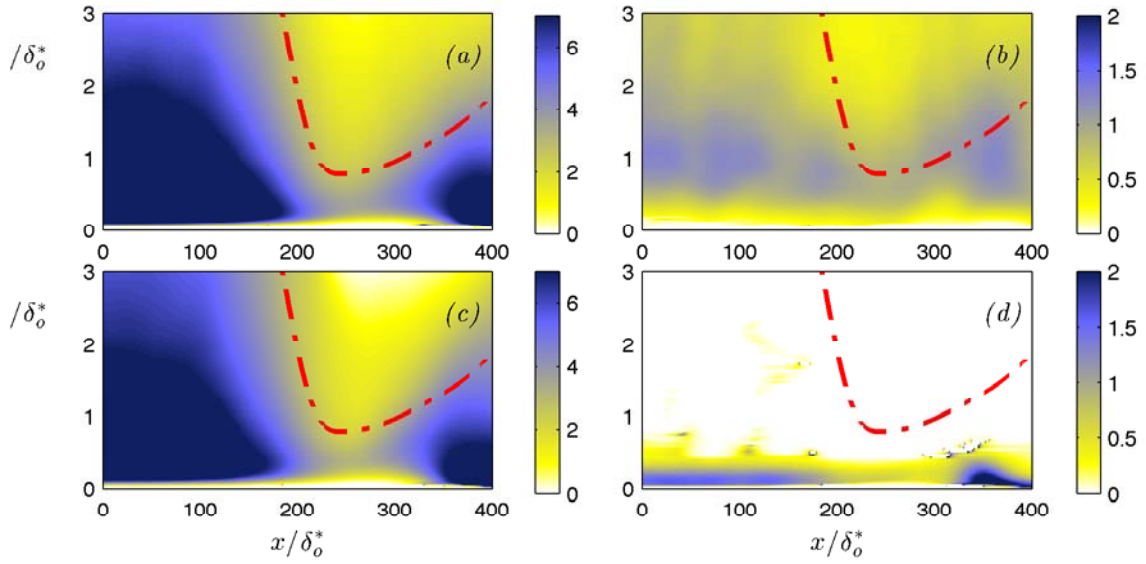


FIG. 11. Frequency of Q2 and Q4 events. Left: all events; right: events with $-u'v' > 4.0u'_{\rm rms}v'_{\rm rms}$.

one in the recovery region. In the zero-pressure-gradient region the areas of strong $v'$ are less elongated than the $u'$ streaks, as is expected in boundary layers. At this height, sweeps are more frequent than ejections. The cross plane shows both sweeps and ejections, as well as the cross-section of quasi-streamwise vortices in the near-wall region. In the high-acceleration region, the picture is quite different; the boundary layer is thinner, but a thick region with very small streamwise velocity gradient can be observed (as shown by the distance between the 90% and 98% boundary-layer thicknesses). Very strong incursions of irrotational fluid from the freestream penetrate the boundary layer and sometimes reach the wall (one such "splatting" events can be seen at $z/\delta_o^* \simeq 14$).

The frequency of the occurrence of Q2 ($u' < 0,\ v' > 0$) and Q4 ($u' > 0,\ v' < 0$) events is shown in Figure 11. The frequency is defined as the inverse of the mean

spanwise separation, $r$, between two events,

$$f(x,y) \equiv \frac{1}{r^+(x,y)} = \frac{n(x,y)}{\Lambda_z^+}, \tag{9}$$

where $n$ is the spanwise count of events, and $\Lambda_z$ is the spanwise domain size. In the normalization used, the figure shows the number of events per 1000 viscous units in $z$. As observed in previous studies,[6,17,20,21] the burst frequency decreases significantly in the acceleration region; however, if we only consider the strong events (those with $-u'v' > 4.0 u'_{\rm rms} v'_{\rm rms}$, where $u'_{i,\rm rms} = \langle u'_i u'_i \rangle^{1/2}$) we notice that the frequency of strong Q4 events initially decreases slightly, but then has a sudden increase (at $x/\delta_o^* \simeq 330$); this is consistent with the occurrence of the strong splatting events and, later, with the appearance of turbulent spots. The spanwise size of the strong Q4 events, shown in Figure 12 and defined as

$$\ell(x,y) \equiv \gamma(x,y)\; r(x,y) \tag{10}$$

(where $\gamma$ is the intermittency, defined as the percentage of the spanwise domain length, $\Lambda_z$, over which the events are observed), also increases in the acceleration region, consistent with the picture described.

### C. Relaminarization mechanisms

In a canonical zero-pressure gradient case, Jimenez and Pinelli[39] showed that the turbulence-generation cycle consists of the generation of streaks by the advection of vortices, and the generation of vortices from the instability of the streaks. They also find that the wall-normal advection of spanwise vorticity, $\langle v' \omega'_z \rangle$ is critical for the generation of streaks. In the present study, the wall-normal velocity is significantly reduced in the acceleration region: the damping of the wall-normal fluctuations may be the reason for the shut-down of the streak-generation mechanism, and the flow relaminarization, consistent with the mechanism proposed by Jimenez and Pinelli.[39]

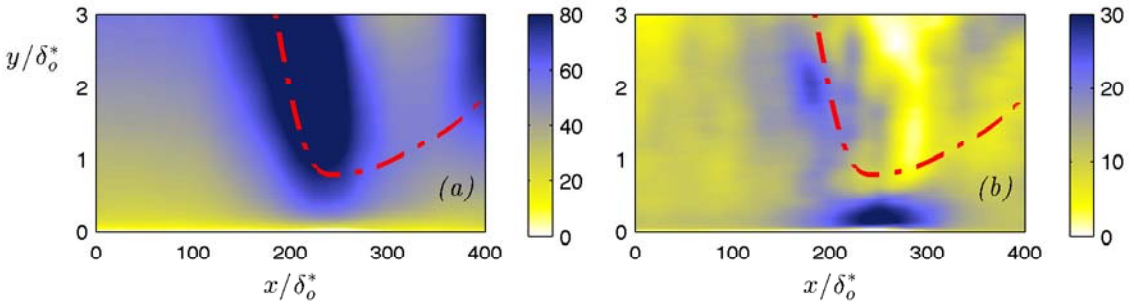


FIG. 12. Average spanwise size of Q4 events, $\ell^+$. Left: all events; right: events with $-u'v' > 4.0u'_{\rm rms}v'_{\rm rms}$.

According to this picture, if the wall-normal component of the velocity is re-energized, relaminarization should not occur. To test this hypothesis, we performed large-eddy simulations of the flow over an accelerating boundary layer, in the same configuration as Case DNS1, replacing the smooth wall with sand-grain roughness. An immersed-boundary method is used to represent the rough surfaces, with the roughness model proposed by Scotti:[40] a virtual sand-paper is constructed from randomly oriented and distributed ellipsoids of the same shape and size (with the three semi-axes equaling $h$, $1.5h$, and $2h$); this model was found to give an equivalent sand-grain roughness height $h_s \approx h$ in the transitionally rough regime.[40] The volume fraction of each cell occupied by the fluid is calculated in pre-processing, and the force exerted by the roughness on the flow is imposed on the right-hand side of the $u_i$-momentum equation to reduce the velocity by an amount proportional to the solid volume in each cell. The force can be directly integrated to obtain the total drag. Implementation details can be found in Yuan.[41] Three simulations were performed (Table I): one with a smooth wall, one with $h_s = 0.2\delta_o^*$ and one with $h_s = 0.4\delta_o^*$. The roughness is very well resolved in the wall-normal direction, more marginally

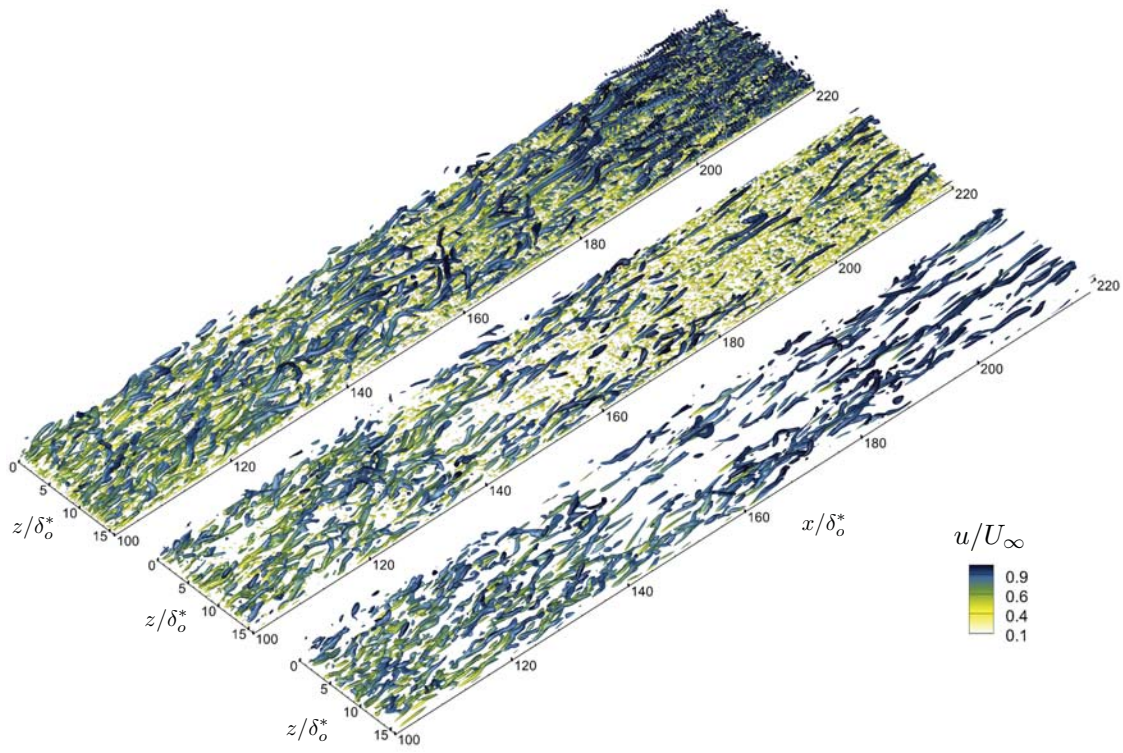


FIG. 13. Isosurfaces of $Q$ colored by $y$. From bottom to top, smooth wall, $h_s = 0.2\delta_o^*$ and $h_s = 0.4\delta_o^*$.

so in the streamwise and spanwise ones (between three and twelve points are used to resolve a roughness element, depending on the value of $h_s$). Numerical studies, however, have shown this number to be sufficient to obtain grid-converged results.

Figure 13 compares isosurfaces of $Q$, colored by $U/U_\infty$, for the three cases. The smooth-wall LES has the same eddy structure observed in the DNS, while the two rough-wall cases have more frequent occurrence of eddies in the high-acceleration region, and a more chaotic appearance. Small structures (yellow in color, light gray in black-and-white) can be observed very near the wall, generated in the wake of the roughness elements. The effect of the roughness elements is to increase

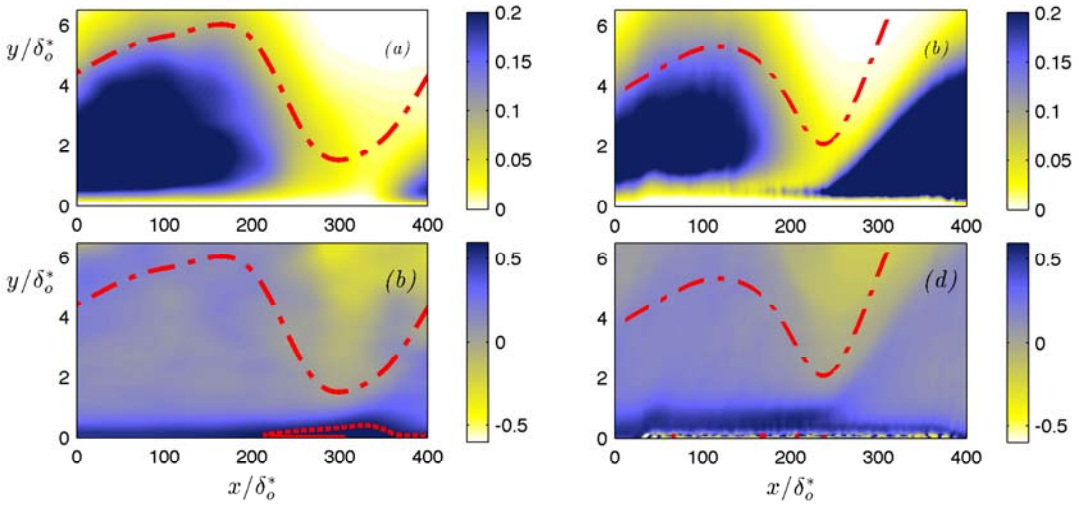


FIG. 14. Contours of *(a-b)* the wall-normal Reynolds stress $\langle v'v' \rangle$ and *(c-d)* anisotropy of the streamwise normal Reynolds stress, $b_{11}$. The dashed line shows contour level 0.6. The dash-dot line shows $\delta_{95}$. The thick line shows the rough surface. *(a,c)* Smooth wall (Case LES1s); *(b,d)* $h_s = 0.4\delta_o^*$ (Case LES1h4).

the wall-normal velocity fluctuations near the wall (Figure 14*(a-b)*), and decrease the Reynolds-stress anisotropy (Figure 14*(c-d)*), which never approaches the 1D-turbulence limit. As a result, the inner-layer turbulence generation mechanism is modified by acceleration only slightly (for $h_s = 0.2\delta_o^*$) or not at all (for $h_s = 0.4\delta_o^*$); the relaminarized-flow region is much reduced, as shown by the distributions of $Re_\theta$ and $C_f$ (Figure 15). The mean velocity profiles (not shown) recover the logarithmic behavior by $x/\delta_o^* \simeq 320$ for the low-roughness case, while in the high-roughness case the log-law slope decreases in the high-acceleration region, but the standard logarithmic behavior is re-established by $x/\delta_o^* \simeq 280$.

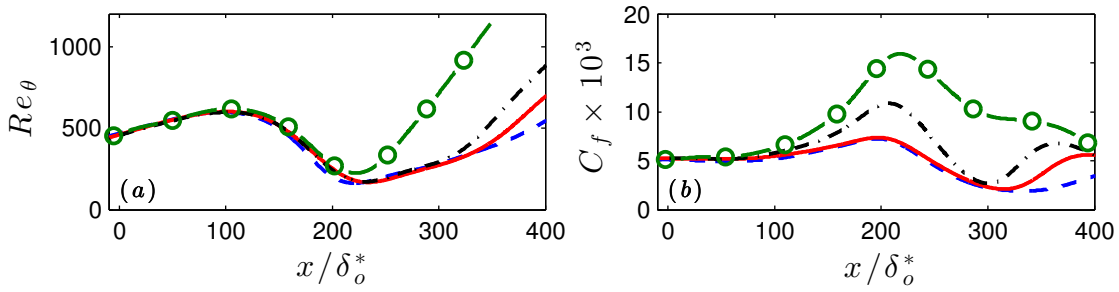


FIG. 15. Boundary layer parameters. *(a)* Reynolds number $Re_\theta$; *(b)* Skin-friction coefficient $C_f$. - - - DNS, smooth; —— LES, smooth; —·— LES, $h_s/\delta_o^* = 0.2$'; —o— LES, $h_s/\delta_o^* = 0.4$'.

### D. Reynolds stress budgets

The transport equation for the Reynolds stresses can be written as[42]

$$0 = -U_k \frac{\partial}{\partial x_k}\langle u_i' u_j' \rangle - \left( \langle u_i' u_k' \rangle \frac{\partial U_j}{\partial x_k} + \langle u_j' u_k' \rangle \frac{\partial U_i}{\partial x_k} \right) - \varepsilon_{ij} - \frac{\partial}{\partial x_k}\langle u_i' u_j' u_k' \rangle$$
$$- \left( \left\langle u_i \frac{\partial p'}{\partial x_j} \right\rangle + \left\langle u_j \frac{\partial p'}{\partial x_i} \right\rangle \right) + \nu \nabla^2 \langle u_i' u_j' \rangle \qquad (11)$$

where the terms in (11) are, from left to right, the mean-flow advection, production, dissipation, turbulent diffusion, pressure work (sum of pressure-velocity gradient and pressure diffusion) and viscous diffusion. The dissipation tensor is given by

$$\varepsilon_{ij} = \nu \left\langle \frac{\partial u_i'}{\partial x_k} \frac{\partial u_j'}{\partial x_k} \right\rangle . \qquad (12)$$

The terms in the budgets of $\langle u'u' \rangle$ and $\langle v'v' \rangle$ are shown in Figures 16 and 17. The budget of $\langle u'u' \rangle$ is canonical in the zero-pressure-gradient region: production and dissipation dominate, turbulent diffusion is important near the wall, and changes sign, and viscous diffusion is important near the wall only. Pressure work (which is mostly due to the pressure diffusion, $\partial \langle u'p' \rangle / \partial x$) is smaller than the other terms but still significant. In the acceleration region both production and dissipation decrease,

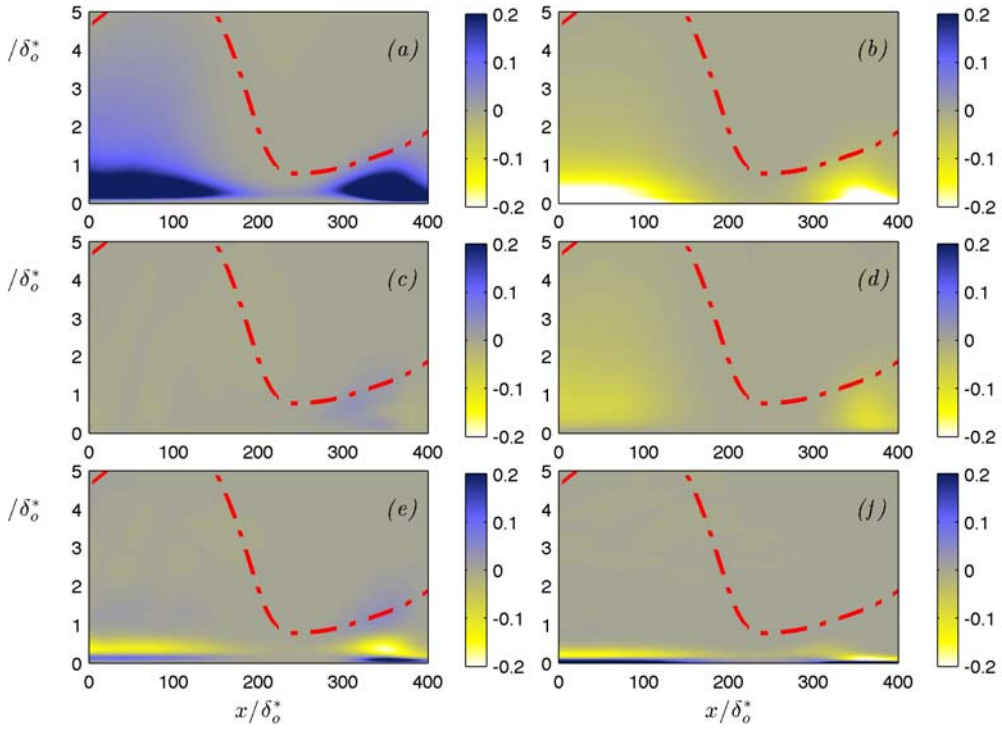


FIG. 16. Budget of $\langle u'u' \rangle$. Case DNS1. All terms are normalized by $u_\tau^4/\nu$. *(a)* Production; *(b)* dissipation; *(c)* mean-flow advection; *(d)* pressure work; *(e)* turbulent diffusion; *(f)* viscous diffusion.

but production remains larger, consistent with experimental data.[15] The decrease of the pressure work is more pronounced: it begins earlier and ends later than the damping of the production term. This can be observed more clearly (because of the difference in the contour levels) in Figure 17. The disappearance of the term that feeds energy into the wall-normal fluctuations (and the similar one in the spanwise term) is the cause for the damping of $v'$ in the strong acceleration region, which appears to be the main cause for the relaminarization of the flow.

To investigate this point further, we consider the decomposition of the pressure

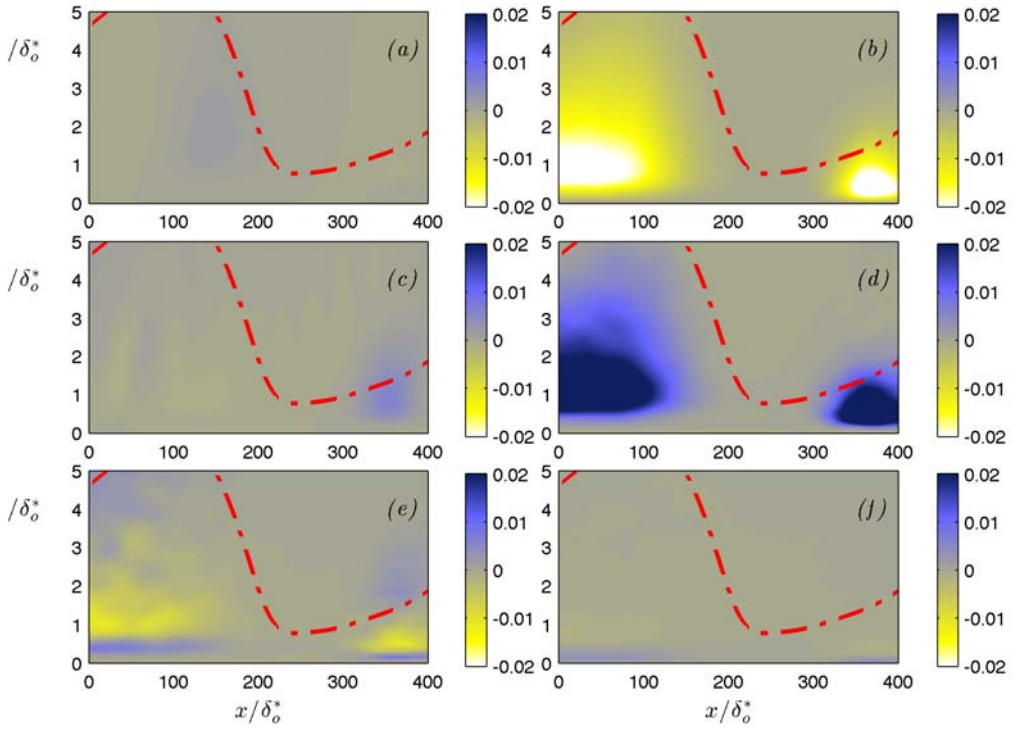


FIG. 17. Budget of $\langle v'v' \rangle$. Case DNS1. All terms are normalized by $u_\tau^4/\nu$. *(a)* Production; *(b)* dissipation; *(c)* mean-flow advection; *(d)* pressure work; *(e)* turbulent diffusion; *(f)* viscous diffusion.

into fast and slow term, $p'_f$ and $p'_s$, respectively, which satisfy the following Poisson equations:

$$p' = p'_f + p'_s; \qquad \nabla^2 p'_f = -2\frac{\partial u'_i}{\partial x_j}\frac{\partial U_j}{\partial x_i}; \qquad \nabla^2 p'_s = -\frac{\partial u'_i}{\partial x_j}\frac{\partial u'_j}{\partial x_i}. \tag{13}$$

Figure 18 shows isosurfaces of the right-hand-side of the two Poisson equations in (13). The slow term resembles the isosurfaces of $Q$ (which is related to the pressure by $Q = \nabla^2 P/2$, Ref. 43): it is concentrated in vortical regions and highlights the quasi-streamwise vortices near the wall, the hairpins in the outer layer. While some decay of the slow-pressure-source term can be observed in the high-acceleration region

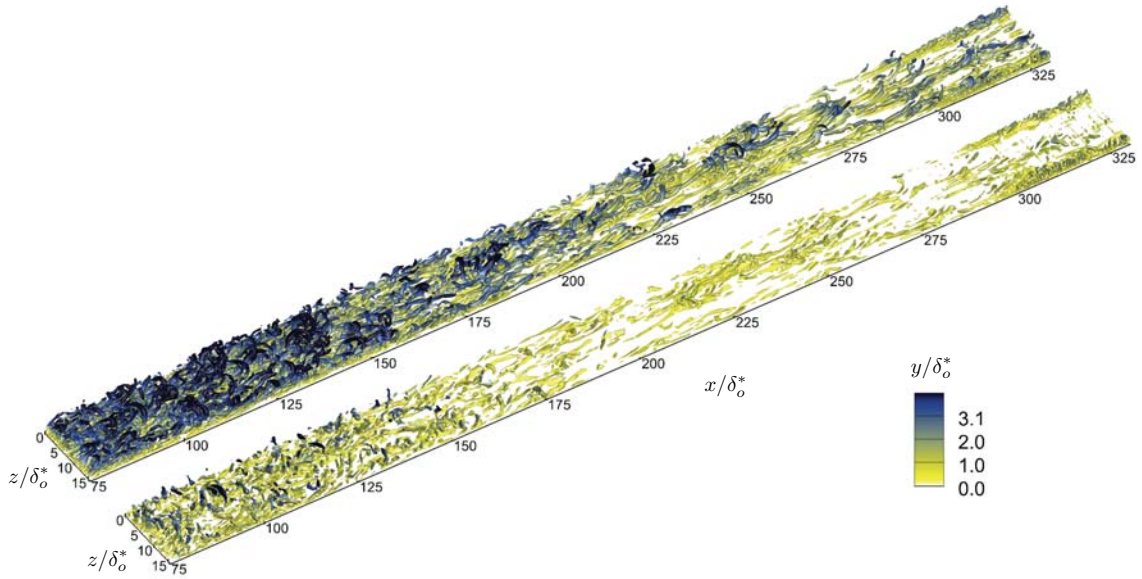


FIG. 18. Isosurfaces of the source term for the pressure-fluctuation equation, (13). Bottom: Fast term; top: slow term. The isosurfaces are colored by the distance from the wall.

($150 < x/\delta_o^* < 250$), this decrease is not nearly as significant as that observed in the fast term. This is consistent with the expectation that the fast term, which depends directly on the mean velocity gradient, reacts more rapidly to perturbations in the mean flow.

As a result of the decrease of the source term in the Poisson equation, the pressure fluctuations do not adapt to the outer-flow acceleration. A region with very low variance of the fluctuating pressure, relative to the local state of the flow, occurs for $300 > x/\delta_o^* > 150$ (Figure 19*(a)*); the streamwise derivative of $p'$ (Figure 19*(b)*) has the same behavior. The damping of the pressure fluctuations due to the effect of the fast pressure appears to be the main reason for the decrease of the pressure work term, that in turn causes the reduction of the wall-normal fluctuations, whose final effect is to cause flow relaminarization.

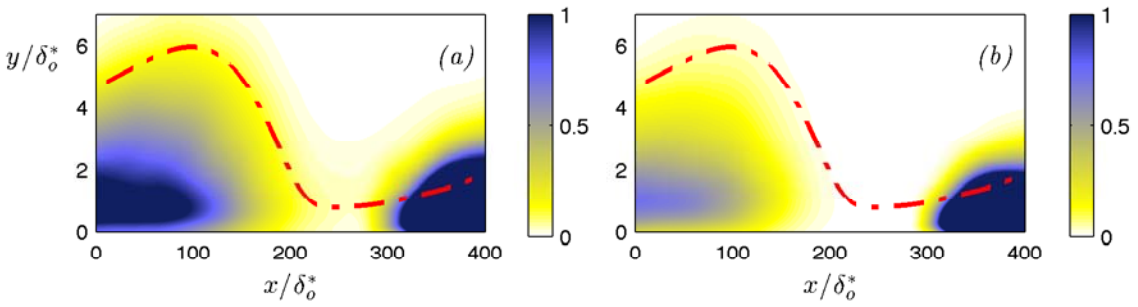


FIG. 19. *(a)* Contours of $100\langle p'p'\rangle$; *(b)* contours of $100\langle(\partial p'/\partial x)^2\rangle$. All quantities are normaled by $u_\tau$ and $\nu$.

## IV. CONCLUSIONS

We have performed numerical simulations of spatially developing boundary layers subjected to favorable pressure gradient (FPG). The acceleration is strong enough that flow relaminarization is expected to occur. We carried out both direct numerical simulations (DNS) and large-eddy simulations (LES) at low Reynolds number, and LES at a higher Reynolds number, to validate the model by comparison with experimental data (which are not available at the lower $Re$). Since the freestream and friction velocities increase by a factor of almost three between inflow and outflow, the simulations have to be over-resolved in the initial region in order to achieve acceptable resolution in the region near the outlet. In all cases, however, the resolution was quite fine, and expected to yield accurate results ($\Delta x^+_{max} = 9$, $\Delta z^+_{max} = 4$ for the DNS and $\Delta x^+_{max} = 70$, $\Delta z^+_{max} = 16$ for the LES).

We observe all the well-documented effects of FPG on the turbulent statistics: the decrease of $C_f$ in the high acceleration region, followed by a recovery to the turbulent value; the disappearance of a logarithmic layer, replaced by a well-mixed region with little or no velocity gradient (and, hence, production); the transition from

a boundary-layer Reynolds stress profile to a sink-flow one, with an upward concavity, followed by the re-establishment of the standard profile of $\langle u'v' \rangle$. Remnants of the re-transition process can still be observed in the recovery region, especially in the form of an overshoot of the total shear stress.

While the streamwise fluctuations preserve their upstream value as fluid particles are advected downstream, the wall-normal and spanwise ones decrease by orders of magnitude, becoming negligible in the high-acceleration region. The shear stress also decreases, as a result of the reduced $v'$ and not, as in many other flows, because of a decorrelation of $u'$ and $v'$ fluctuations. The Reynolds-stress anisotropy is significantly increased in the high-acceleration region: the $v'$ fluctuations are reduced much more than the streamwise ones, and the flow tends towards the 1D turbulence limit, with values of the anisotropy $b_{11}$ approaching 2/3.

The coherent eddies, in the high acceleration region, become less frequent, and the near-wall flow less turbulent: the streaks are longer and more stable, the coherent vortices are reoriented in the streamwise direction by the mean strain, and the streamwise vorticity $\omega_x'$ becomes dominant, and mainly concentrated in the quasi-streamwise vortices. The leftover turbulence, however, plays a role in the re-transition process: once the acceleration ends, turbulent spots appear, which grow as they are advected downstream, eventually filling the entire boundary layer. This process is also reminiscent of freestream-turbulence-induced boundary-layer transition.

The decrease in the burst frequency observed by several researchers was also seen here, but does not extend to very strong Q4 events, whose frequency remains constant through most of the acceleration region, and even increases towards its end. The spanwise extent of these events also increases; they are mostly due to incursions of outer-layer, irrotational fluid that penetrate into the boundary layer and impinge the wall.

We also performed simulations of the same flow over a roughened wall, to determine the importance of the $v'$ fluctuations in the relaminarization process. In the rough-wall case, the wall-normal fluctuations are amplified by the presence of the roughness elements, which induce local stagnation regions upstream of the element, and flow separation downstream of it. The increased $v'$ fluctuations result in more isotropic near-wall turbulence, a more disturbed inner layer, and either a complete lack of relaminarization or (for low roughness) an early re-establishment of the equilibrium turbulent flow, as indicated by $C_f$ and mean velocity profiles.

The Reynolds stress budgets highlight an important effect of the acceleration: the energy redistribution term becomes very small in the strong-acceleration region. This is due to a significant reduction of the source term in the Poisson equation for the fast pressure term; as a result, the pressure fluctuations do not catch up to the mean-flow dynamic pressure $\rho U_\infty^2/2$, nor to the near-wall pressure scale $\rho u_\tau^2/2$. The decrease of the energy redistribution causes the damping of the wall-normal and spanwise fluctuations; the streamwise ones, which have a separate production term, do not decay (although they also do not catch up to the freestream energy).

Based on the simulation results, we propose the following sequence of events leading to relaminarization in highly accelerated flows: first, the pressure fluctuations are reduced due to the effect of the mean flow on the fast-pressure term; this phenomenon begins as soon as the freestream velocity increases. The decrease of the pressure fluctuations causes the energy redistribution term to become negligible, thus damping $v'$ and $w'$ fluctuations. The beginning of the reduction in $v'$ and $w'$ almost coincides with the decrease of the energy redistribution and pressure fluctuations. The $u'$ fluctuations, on the other hand, do not decay significantly, since the production decrease lags the decrease of the pressure work: they remain nearly constant as they are advected from upstream. The Reynolds shear stress also decay (although at a slower rate than $v'$) due to the very significant decrease of the wall-normal

fluctuations. The $v'$ fluctuations are responsible for the wall-normal advection of spanwise vorticity that has been shown to be critical for the generation and instability of streaks;[39] their reduction causes the streaks to be stabilized and the flow to relaminarize. In the present simulation the acceleration extended for approximately $250\delta_o^*$ (about 50 boundary layer thicknesses). Over this distance, dissipation did not decrease the $\langle u'u' \rangle$ stresses appreciably, and when acceleration ended the flow retransitioned quickly. If the acceleration were sustained for a longer distance, this process might be different, and retransition might occur more slowly. In aeronautical applications (in which the Reynolds number is very high) this may not occur frequently, but in internal flow it might be more significant.

## ACKNOWLEDGMENTS

This research was supported by the Natural Sciences and Engineering Research Council (NSERC) under the Discovery Grant program. The authors thank the High Performance Computing Virtual Laboratory (HPCVL), Queen's University site, for the computational support. UP also acknowledges the support of the Canada Research Chairs Program.

## REFERENCES

[1]R. Narasimha and K. R. Sreenivasan, "Relaminarization of fluid flows," in *Adv. Applied Mech.*, Vol. 19 (Academic Press Professional, Inc., New York, 1979) pp. 221–309.

[2]K. R. Sreenivasan, "Laminarescent, relaminarizing and retransitional flows," Acta Mechanica **44**, 1–48 (1982).

[3]H. Schlichting, *Boundary-Layer Theory* (McGraw-Hill, New York, 1979).

[4]B. E. Launder and W. P. Jones, "Sink flow turbulent boundary layers," J. Fluid Mech. **38**, 817–831 (1969).

[5]W. P. Jones and B. E. Launder, "Some properties of sink-flow turbulent boundary layers," J. Fluid Mech. **56**, 337–351 (1972).

[6]M. A. Badri Narayanan and V. Ramjee, "On the criteria for reverse transition in a two-dimensional boundary layer flow," J. Fluid Mech. **35**, 225–241 (1969).

[7]P. Spalart, "Numerical study of sink-flow boundary layers," J. Fluid Mech. **172**, 307–328 (1986).

[8]B. E. Launder, "Laminarization of the turbulent boundary layer in a severe acceleration," J. Appl. Mech. **31**, 707—708 (1964).

[9]B. E. Launder, "Laminarization of the turbulent boundary layer by acceleration," Tech. Rep. (M.I.T. Gas Turbines Lab. Rep. No. 77, 1964).

[10]S. J. Kline, W. C. Reynolds, F. A. Schraub, and P. W. Runstadler, "The structure of turbulent boundary layers," J. Fluid Mech. **30**, 741–773 (1967).

[11]R. F. Blackwelder and L. S. G. Kovasznay, "Large-scale motion of a turbulent boundary layer during relaminarization," J. Fluid Mech. **53**, 61–83 (1972).

[12]F. A. Schraub and S. J. Kline, "A study of the structures of the turbulent boundary layer with and without longitudinal pressure gradients," Report No. MD-12 (Thermoscience Div., Stanford Univ., 1965).

[13]V. C. Patel and M. R. Head, "Reversion of turbulent to laminar flow," J. Fluid Mech. **34**, 371–392 (1968).

[14]R. Narasimha and K. R. Sreenivasan, "Relaminarization in highly accelerated turbulent boundary layers," J. Fluid Mech. **61**, 417–447 (1973).

[15]M. A. Badri-Narayanan, S. Rajagopalan, and R. Narasimha, "Some experiments on the fine structure of turbulence," Report No. FM 15 (Dept. Aero. Eng., Ind. Inst. Sci., 1974).

[16]H. D. Murphy, F. W. Chambers, and D. M. McEligot, "Laterally converging duct flows. Part 1. Mean flow," J. Fluid Mech. **127**, 379—401 (1983).

[17]F. W. Chambers, H. D. Murphy, and D. M. McEligot, "Laterally converging duct flows. Part 2. Temporal wall shear stress," J. Fluid Mech. **127** (1983).

[18]D. M. McEligot and H. Eckelmann, "Laterally converging duct flows. Part 3. Mean turbulence structure in the viscous layer," J. Fluid Mech. **549**, 233—273 (2006).

[19]D. M. McEligot, R. S. Brodkey, and H. Eckelmann, "Laterally converging duct flows. Part 4. Temporal behaviour in the viscous layer," J. Fluid Mech. **634**, 433—461 (2009).

[20]H. H. Fernholz and D. Warnack, "The effects of a favourable pressure gradient and of the Reynolds number on an incompressible axisymmetric turbulent boundary layer. Part 1. The turbulent boundary layer," J. Fluid Mech. **359**, 329–356 (1998).

[21]D. Warnack and H. H. Fernholz, "The effects of a favourable pressure gradient and of the Reynolds number on an incompressible axisymmetric turbulent boundary layer. Part 2. The boundary layer with relaminarization," J. Fluid Mech. **359**, 357–371 (1998).

[22]M. P. Escudier, A. Abdel-Hameed, M. W. Johnson, and C. J. Sutcliffe, "Laminarisation and re-transition of a turbulent boundary layer subjected to favourable pressure gradient," Exp. Fluids **25**, 491–502 (1998).

[23]C. Bourassa and F. O. Thomas, "An experimental investigation of a highly accelerated turbulent boundary layer," J. Fluid Mech. **634**, 359–404 (2009).

[24]U. Piomelli, E. Balaras, and A. Pascarelli, "Turbulent structures in accelerating boundary layers," J. Turbul. **1**, 001–1–16 (2000).

[25]G. De Prisco, A. Keating, and U. Piomelli, "Large-eddy simulation of accelerating boundary layers," *AIAA Paper 2007-0725* (2007).

[26]Z. Harun, J. P. Monty, R. Mathis, and I. Marusic, "Pressure gradient effects on the large-scale structure of turbulent boundary layers," J. Fluid Mech. **715**, 477—498

(2013).

[27]M. Germano, U. Piomelli, P. Moin, and W. H. Cabot, "A dynamic subgrid-scale eddy viscosity model," Phys. Fluids A **3**, 1760–1765 (1991).

[28]D. K. Lilly, "A proposed modification of the Germano subgrid-scale closure method," Phys. Fluids A **4**, 633–635 (1992).

[29]C. Meneveau, T. S. Lund, and W. H. Cabot, "A Lagrangian dynamic subgrid-scale model of turbulence," J. Fluid Mech. **319**, 353–385 (1996).

[30]A. J. Chorin, "Numerical solution of Navier-Stokes equations," Math. Comput. **22**, 745–762 (1968).

[31]J. Kim and P. Moin, "Application of a fractional step method to incompressible Navier-Stokes equations," J. Comput. Phys. **59**, 308–323 (1985).

[32]Y. Morinishi, T. S. Lund, O. V. Vasilyev, and P. Moin, "Fully conservative higher order finite difference schemes for incompressible flows," J. Comput. Phys. **143**, 90–124 (1998).

[33]A. Keating, U. Piomelli, E. Balaras, and H.-J. Kaltenbach, "A priori and a posteriori tests of inflow conditions for large-eddy simulation," Phys. Fluids **16**, 4696–4712 (2004).

[34]A. Keating, U. Piomelli, K. Bremhorst, and S. Nešić, "Large-eddy simulation of heat transfer downstream of a backward-facing step," J. Turbul. **5**, 20–1–27 (2004).

[35]A. Keating and U. Piomelli, "A dynamic stochastic forcing method as a wall-layer model for large-eddy simulation," J. Turbul. **7**, 12–1–24 (2006).

[36]T. S. Lund, X. Wu, and K. D. Squires, "Generation of inflow data for spatially-developing boundary layer simulations," J. Comput. Phys. **140**, 233–258 (1998).

[37]I. Orlanski, "A simple boundary condition for unbounded hyperbolic flows," J. Comput. Phys. **21**, 251–269 (1976).

[38]X. Wu and P. Moin, "Direct numerical simulation of turbulence in a nominally zero-pressure-gradient flat-plate boundary layer," J. Fluid Mech. **630**, 5–41 (2009).

[39]J. Jiménez and A. Pinelli, "The autonomous cycle of near-wall turbulence," J. Fluid Mech. **389**, 335–359 (1999).

[40]A. Scotti, "Direct numerical simulation of turbulent channel flows with boundary roughened with virtual sandpaper," Phys. Fluids **18**, 031701 (2006).

[41]J. Yuan, *Large-eddy simulations of accelerating boundary-layer flows over rough surfaces*, Master's thesis, Queen's University (2011).

[42]P. S. Bernard and J. M. Wallace, *Turbulent Flow: Analysis, Measurement, and Prediction* (Wiley, Hoboken, NJ, 2002).

[43]Y. Dubief and F. Delcayre, "On coherent vortex identification in turbulence," J. Turbul. **1**, 011–1—22 (2000).